

Dual-band switchable mid-infrared emitter based on In_3SbTe_2 for gas detection application

Biyuan Wu(吴必园), Xiqiao Huang(黄希桥), and Xiaohu Wu(吴小虎)
Citatio: Chin. Phys. B, 2025, 34 (**9**): 094403. DOI: 10.1088/1674-1056/ade59e
http://cpb.iphy.ac.cn; http://iopscience.iop.org/cpb

What follows is a list of articles you may be interested in

Experimental study on the regulation of radiative heat flux by coating SiC film

Haifeng Xia(閤海峰) and Huihui Sun(孙慧慧)
Chin. Phys. B, 2025, 34 (**5**): 054402. DOI: 10.1088/1674-1056/adbee0

Influence of substrate effect on near-field radiative modulator based on biaxial hyperbolic materials

Ruiyi Liu(刘睿一), Haotuo Liu(刘皓佗), Yang Hu(胡杨), Zheng Cui(崔峥), and Xiaohu Wu(吴小虎)
Chin. Phys. B, 2024, 33 (**4**): 044403. DOI: 10.1088/1674-1056/ad2a6c

Preparation and cooling performance analysis of double-layer radiative cooling hybrid coatings with $TiO_2/SiO_2/Si_3N_4$ micron particles

Yang-Chun Zhao(赵洋春) and Yong-Min Zhou(周勇敏)
Chin. Phys. B, 2023, 32 (**11**): 114401. DOI: 10.1088/1674-1056/acdac0

Tuning infrared absorption in hyperbolic polaritons coated silk fibril composite

Lihong Shi(史丽弘) and Jiebin Peng(彭洁彬)
Chin. Phys. B, 2022, 31 (**11**): 114401. DOI: 10.1088/1674-1056/ac8cdc

Calculation of radiative heat flux on irregular boundaries in participating media

Yu-Jia Sun(孙玉佳) and Shu Zheng(郑树)
Chin. Phys. B, 2020, 29 (**12**): 124401. DOI: 10.1088/1674-1056/abb22a

---

SPECIAL TOPIC — Heat conduction and its related interdisciplinary areas

Dual-band switchable mid-infrared emitter based on In_3SbTe_2 for gas detection application

Biyuan Wu(吴必园)[1,2], Xiqiao Huang(黄希桥)[2], and Xiaohu Wu(吴小虎)[1,†]

[1] *Thermal Science Research Center, Shandong Institute of Advanced Technology, Jinan* 250100, *China*
[2] *School of Power and Energy, Northwestern Polytechnical University, Xi'an* 710072, *China*

(Received 21 April 2025; revised manuscript received 5 June 2025; accepted manuscript online 18 June 2025)

As a highly energy-efficient and sensitive radiation source, narrowband thermal emitters provide an ideal solution for non-contact gas detection, enabling the widespread application of mid-infrared "molecular fingerprint" technology. However, most narrowband thermal emitters lack reconfigurability, limiting their adaptability in practical applications. In this study, we propose a novel dual-band switchable narrowband thermal emitter in the mid-infrared region. The emitter consists of an aperiodic Ge/SiO_2/Ge/SiO_2 (GSGS) structure and a phase change material In_3SbTe_2 (IST). When IST is in the crystalline state, the emitter achieves narrowband emission peaks at wavelengths of 3.79 μm and 6.12 μm, corresponding to the "on" state. However, when IST transitions to the amorphous state, the dual-band high emission disappears and it features angle- and polarization-independent behavior, representing the "off" state. Furthermore, we verify the physical mechanism behind the high emission through phase and amplitude calculations as well as electric field distribution analysis. Notably, the introduction of the IST provides an additional degree of freedom for tunability. Furthermore, by adjusting the thickness of the spacer layer, the emitter can be precisely tuned to match the characteristic absorption peaks of various mid-infrared gases, such as CH_4, CO_2, CO, and NO, enabling multi-gas detection in mixed gas environments. The proposed thermal emitter serves as an effective and low-cost alternative for dual-band narrowband mid-infrared light sources, contributing to the advancement of multi-gas detection strategies.

Keywords: dual-band emitter, switchable, In_3SbTe_2, multi-gas detection

PACS: 44.40.+a, 52.25.Os, 91.60.Hg

DOI: 10.1088/1674-1056/ade59e **CSTR:** 32038.14.CPB.ade59e

1. Introduction

With the rapid progression of industrialization and the intensifying challenges posed by environmental pollution, the demand for advanced gas sensing technologies has surged across a spectrum of critical domains, including environmental monitoring,[1,2] industrial safety,[3,4] and medical diagnostics.[5,6] Among these, non-contact gas sensing has emerged as a particularly promising approach, owing to its exceptional sensitivity, rapid response times, and non-invasive nature.[7] The mid-infrared (MIR) spectral region holds particular significance in chemical sensing, as it encompasses the fundamental vibrational absorption bands of numerous molecular bonds, thereby enabling highly specific and unambiguous gas identification.[8,9] In contrast to optical fiber gas sensors[10–12] and semiconductor-based sensors,[13,14] non-dispersive infrared (NDIR) technology operates by quantifying the attenuation of infrared light as it traverses a gas cell containing the target analyte.[15] Through meticulous analysis of the resultant intensity variations, NDIR sensors facilitate not only the precise determination of gas composition and concentration, but also the capture of distinct vibrational and rotational spectral signatures of molecular species within the MIR range. These unique spectral features, often termed "molecular fingerprints", provide a robust and highly specific foundation for gas detection.[16–18]

Traditionally, quantum cascade lasers (QCLs) have been widely employed as light sources in NDIR technology due to their high output power and exceptional spectral purity.[19,20] However, QCLs operate based on intersubband transitions, necessitating precise fabrication techniques and stringent energy level control when used as the primary light source for gas sensing. While QCLs demonstrate outstanding performance in gas detection, their high manufacturing costs and the complexity of energy level management hinder their integration into portable and highly miniaturized devices. Alternatively, broadband light sources offer a more cost-effective solution.[21] However, their excessive emission can introduce signal interference, significantly compromising detection accuracy, particularly in trace gas sensing applications.

Additionally, thermal emitters based on Kirchhoff's law have also been employed as light sources in NDIR technology, leveraging the principle of selective infrared absorption.[22–30] In general, a higher quality factor (Q-factor) corresponds to a narrower emission bandwidth, which enhances the precision

†Corresponding author. E-mail: wuxiaohu@pku.edu.cn

© 2025 Chinese Physical Society and IOP Publishing Ltd. All rights, including for text and data mining, AI training, and similar technologies, are reserved.

of molecular fingerprint identification and holds promise for trace gas analysis. In recent years, metasurface-based thermal emitters have gained increasing attention.[31–36] Sun *et al.*[36] proposed a mid-infrared thermal emitter based on an all-dielectric metasurface composed of a zigzag array of germanium elliptical disks, achieving narrowband thermal radiation with a high Q-factor. These engineered structures enable precise control over thermal emission properties, allowing their emission spectra to be tailored to match the "molecular fingerprints" of target gases. Therefore, these structures can facilitate gas detection through attenuation-based intensity measurements. However, their fabrication typically relies on intricate nanofabrication techniques, such as lithography and nanoscale etching, which pose significant challenges for large-scale implementation and practical deployment.

To address these challenges, lithography-free multilayer thin-film emitters based on Tamm plasmon polaritons have been proposed.[37–40] For instance, the narrowband mid-infrared thermal emitter based on Tamm plasmon polaritons introduced by Zhu *et al.*[37] eliminates the need for complex micro/nanofabrication techniques while maintaining the Q-factor essential for gas sensing. These advantages lay the foundation for chip-based gas sensors, positioning multilayer thin-film thermal emitters as one of the most promising solutions for practical applications. However, these emitters are commonly designed with metal substrates such as gold or silver, which greatly limit the tunability of their spectrum.

In this paper, we present a novel infrared dual-band narrowband switchable thermal emitter based on the phase change material In_3SbTe_2 (IST). The proposed emitter consists of an alternating deposition of Ge and SiO_2 thin films on an IST substrate. At the optimized thickness, the emission spectra of the emitter are calculated under both crystalline and amorphous states of IST, demonstrating dual-band narrowband thermal emission at wavelengths 3.79 μm and 6.13 μm, respectively. The physical mechanism underlying the dual-band emission is analyzed by electric field distributions. Furthermore, the effects of the incident angle, IST thickness, and spacer layer thickness on the emitter's performance are systematically investigated. Finally, the potential application of the proposed structure in gas sensing is also explored. The proposed thermal emitter provides a low-cost, high-precision solution for gas sensing while also laying the foundation for the future development of multifunctional and reconfigurable photonic devices.

2. Model and method

As depicted in Fig. 1(a), the thermal emitter is composed of a Ge/SiO_2 stack and a phase change material IST. The layer thicknesses of the Ge/SiO_2 stack are denoted as H_1, H_2, H_3, and H_4, while the dielectric constants of Ge and SiO_2 are referenced from Refs. [41,42], respectively. IST is a non-volatile phase change material, and its permittivity is obtained from Ref. [43]. The permittivity of IST is shown in Fig. 1(b). Notably, the permittivity of IST is negative in the crystalline state (cIST), imparting metal-like characteristics. In contrast, in the amorphous state (aIST), the permittivity is positive, exhibiting dielectric properties. Furthermore, substantial differences are observed between the imaginary parts of the aIST and cIST permittivities. IST provides an additional degree of freedom for reconfigurable thermal emission, enabling dynamic control through actively induced phase transitions. In this paper, the spectral reflection (R) and transmission (T) are calculated using the transfer matrix method (TMM). Since the materials used are all reciprocal, the spectral emission (ε) in a given direction is equal to the spectral absorption (A). Thus, there is $\varepsilon = A = 1 - R - T$.

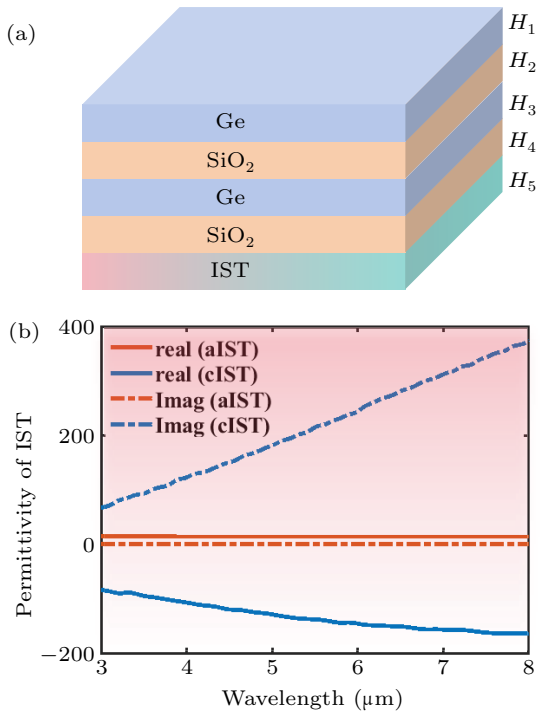


Fig. 1. (a) Schematic diagram of the dual-band narrowband emitter. (b) The permittivity of the IST at different states.

3. Results and discussion

Here, the optimal structural parameters are $H_1 = 0.34$ μm, $H_2 = 1.0$ μm, $H_3 = 0.08$ μm, $H_4 = 2.63$ μm, and $H_5 = 0.08$ μm. The thickness of each layer in the proposed structure was determined by combining the TMM with parameter scanning, with the goal of enabling switchable narrowband thermal emission. Figure 2 presents the spectrum of the proposed dual-band emitter in the 3–8 μm wavelength range. In the crystalline state of IST, the narrowband thermal radiation is achieved at wavelengths 3.79 μm and 6.13 μm, with corresponding emissivities 0.96 and 0.97. However, in the

amorphous state of IST, the emission remains consistently low across the entire wavelength range, nearly approaching zero. This demonstrates that the proposed dual-band thermal emitter can effectively switch between "on" and "off" states through phase transition in IST.

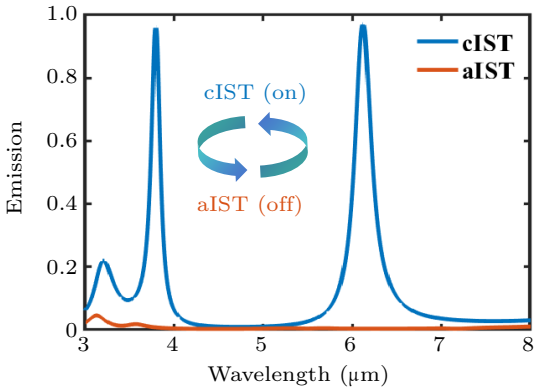


Fig. 2. The emission spectrum of the emitter for cIST and aIST.

The Q-factor is a key metric for evaluating the performance of narrowband thermal emitters and is defined as the ratio between the resonant wavelength and the full width at half maximum (FWHM). Calculated Q-factors of the proposed emitter at the two resonant wavelengths (3.79 μm and 6.13 μm) are approximately 33 and 26, respectively. A performance comparison with recently reported mid-infrared narrowband emitters is summarized in Table 1. The structure exhibits superior Q-factors compared to those reported in Refs. [24,33]. Although Ref. [32] achieves higher Q-factors, its performance relies on independent excitation under TE and TM polarization states, rather than achieving dual-band emission under a single polarization. Overall, the proposed emitter demonstrates competitive performance, particularly in maintaining relatively high Q-factors while simultaneously achieving dual-band thermal emission.

Table 1. Comparison with the performance of narrowband emitters.

References	λ_1 (μm)	Q_1	λ_2 (μm)	Q_2
Ref. [32]	4.28 (TE)	126	5.27 (TM)	51
Ref. [24]	3.69	15.7	–	–
Ref. [33]	4.283	15.77	4.227	18.51
This work	3.79	33	6.13	26

To gain a better understanding of the dual-band high emission behavior in the cIST state, the distributions of the electric field at the wavelengths corresponding to the two emission peaks in the crystalline IST state are calculated, as shown in Fig. 3. The white solid lines in the figure represent the boundaries of each layer in the emitter structure. At a wavelength of 3.79 μm, the electric field exhibits significant enhancement predominantly within the two SiO_2 thin films. Notably, a periodic enhancement pattern appears in the SiO_2 layer adjacent to IST. In contrast, at a wavelength of 6.13 μm, the electric field becomes localized primarily in the upper SiO_2 layer and the intermediate Ge layer. The dual narrowband thermal emission originates from interference effects caused by multiple interfaces and varying optical thicknesses within the Ge/SiO_2/Ge/SiO_2/cIST multilayer structure.

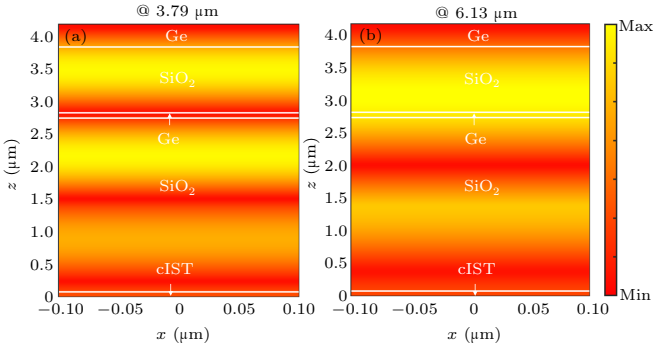


Fig. 3. The distributions of the electronic field at the wavelengths of (a) 3.79 μm and (b) 6.13 μm.

Although we have achieved a dual-band narrowband emitter, as shown in Fig. 2, the emission wavelengths of this emitter remain fixed. Given that absorption peaks of different gases in the mid-infrared region occur at distinct wavelengths, we introduce a SiO_2 spacer layer between the Ge/SiO_2/Ge/SiO_2 (GSGS) structure and the IST film to enhance the emitter's adaptability for gas sensing applications. Figures 4(b) and S1(a) illustrate the emission spectra as a function of the spacer layer thickness in the cIST and aIST states, respectively. In the cIST state, a pronounced redshift of the two primary emission peaks is observed as the spacer layer thickness increases. Furthermore, when the spacer layer thickness exceeds 0.5 μm, a third emission peak emerges, which also redshifts with increasing thickness. By contrast, in the aIST state, the emission remains consistently low across the entire spectral range examined, demonstrating the emitter's excellent switchable functionality. The thickness of the IST layer is a critical parameter in achieving switchable thermal radiation, requiring a careful balance of competing factors. On one hand, the IST must be sufficiently thick in the crystalline state to exhibit metallic characteristics, thereby enabling the emergence of dual-band emission peaks. On the other hand, the IST should remain as thin as possible to ensure that laser annealing can induce a phase transition throughout the entire layer, thereby enabling dynamic reconfigurability. To elucidate this interplay, we systematically investigate the impact of IST thickness on emitter performance across different states, as illustrated in Figs. 4(c) and S1(b). As shown in Fig. 4(c), when the cIST thickness is below 0.015 μm, the proposed emitter is unable to achieve strong emission. As the thickness of cIST increases, the dual narrowband emission peaks gradually appear. When the thickness of IST exceeds 0.05 μm, the strong dual-band thermal emission is consistently maintained. This finding demonstrates that our proposed structure can achieve dual-band thermal emission even with relatively

thin IST layers. Moreover, we examine the dependence of emission on phase-transition layer thickness in the aIST state. The results reveal that the emission remains consistently low across the entire range investigated, in agreement with theoretical expectations. This confirms that the switchable nature of the emitter is governed solely by the optical properties of IST before and after the phase transition, rather than by its thickness.

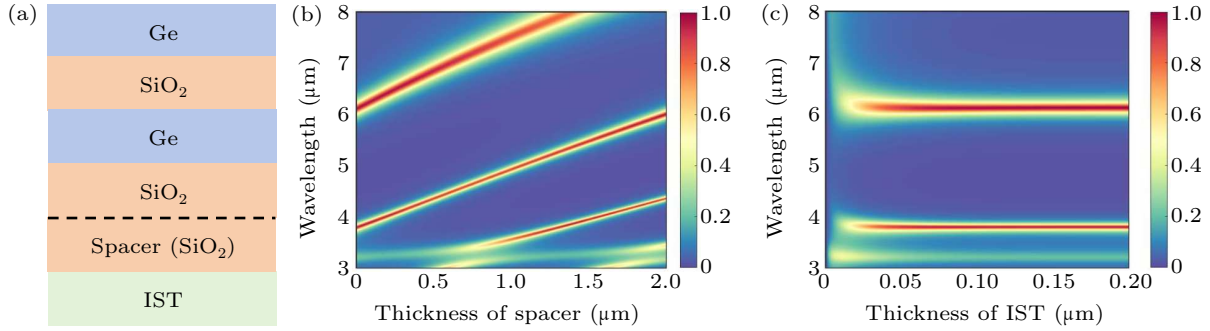


Fig. 4. (a) Schematic illustration of the structure with the introduced spacer layer. (b) Influence of the spacer layer thickness and (c) IST thickness on emission in the cIST state.

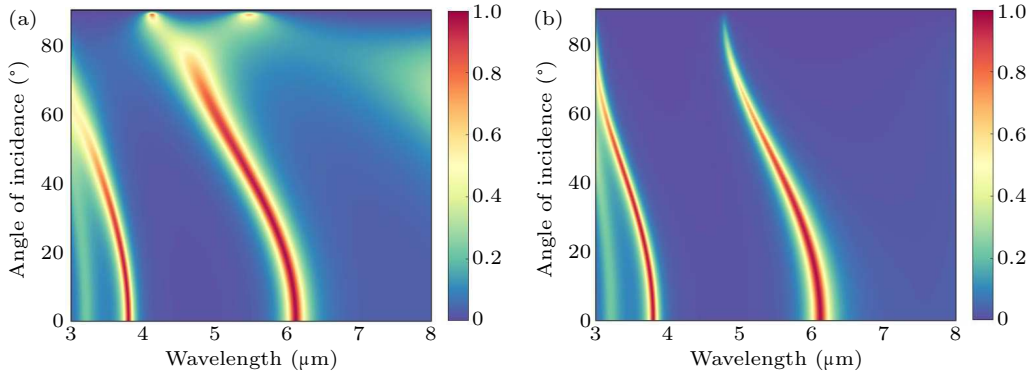


Fig. 5. The effect of the incident angle on the emission of (a) TM and (b) TE waves at cIST state, respectively.

In addition, we examine the impact of the incident angle on the performance of the switchable narrowband emitter, as shown in Fig. 5. Figures 5(a) and 5(b) present the cases for TM and TE wave incidence in the cIST state, respectively. It is found that the response is identical for both TE and TM waves under normal incidence. However, as the incident angle increases, this optical degeneracy is broken, leading to distinct radiative characteristics. In the cIST state, both emission peaks shift toward shorter wavelengths as the incident angle increases. Under normal incidence, the phase change in each layer is $\phi = 2\pi nd/\lambda$, while at an incident angle θ, the phase change becomes $\phi = 2\pi nd\cos\theta/\lambda$. To satisfy the phase-matching condition for resonance, the resonance wavelength decreases with increasing incident angle, resulting in a blue shift of the emission spectrum. Moreover, the emitter exhibits robustness to the incident angle, maintaining high emission up to 70°. However, as the angle increases further, the full width at half maximum also broadens. In the cIST state, the emission spectrum also undergoes a blue shift when a TE wave is incident, which is similar to the behavior observed for TM waves, with only slight differences at large angles. In contrast, in the aIST state (Fig. S2), both TE and TM waves maintain low emission, unaffected by the polarization state of the incident wave.

Table 2. Emission peak positions and corresponding target gases for different spacer layer thicknesses.

H_{Spacer} (μm)	λ_1 (μm)	Gas 1	λ_2 (μm)	Gas 2
0.82	4.7	CO	7.35	–
4.29	4.3	CO_2	6.79	–
1.12	7.69	CH_4	5.16	NO_2
0.61	4.47	CO_2	7.01	H_2O

4. Applications

Finally, we discuss the potential applications of the proposed dual narrowband thermal emitter in gas detection. In Fig. 4, we investigate the ability of the spacer layer thickness to tune both the intensity and position of the emission peaks, providing the possibility of matching the absorption peaks of various gases in the mid-infrared region. Table 2 presents the positions of the two emission peaks at different spacer layer thicknesses, along with the corresponding gases that can be matched.

In the table, H_{Spacer} represents the thickness of the spacer layer SiO_2. It can be observed that when the spacer layer thickness is 0.82 μm and 4.29 μm, the designed emitter can be used

for detecting CO and CO_2, respectively. When the thickness is 1.12 μm, the two emission peaks are located at wavelengths of 7.69 μm and 5.16 μm, which are very close to the absorption peaks of CH_4 and NO_2, making it suitable for detecting these two gases. Additionally, when the thickness is 0.61 μm, the emitter can be utilized for the detection of CO_2 and H_2O. The results indicate that by tuning the spacer layer thickness, selective detection of target gases can be achieved, offering a potential solution for multi-gas sensing applications.

5. Conclusion

In conclusion, we propose a dual-band narrowband switchable thermal emitter for mid-infrared gas detection. In the cIST, the emitter achieves dual-band high emission at wavelengths 3.79 μm and 6.13 μm, with emissivities of 0.96 and 0.97, respectively. However, in the aIST, the high emission properties disappear, demonstrating a significant switchable functionality that can reduce energy consumption for gas detection. Furthermore, the electric field distributions at the resonance wavelengths further confirm the physical mechanism. Notably, the emitter maintains excellent narrowband emission performance at large angles for both TE and TM waves. Additionally, the introduction of a spacer layer provides extra tunability for the emission peak's position and intensity, enabling precise matching with characteristic absorption peaks of various mid-infrared gases, such as CH_4, CO_2, CO, and NO, allowing for multi-gas detection. Overall, the proposed thermal emitter offers low cost, large-area fabrication, and high sensitivity, providing an effective solution for efficient mid-infrared gas detection.

Acknowledgments

This project was supported by the National Natural Science Foundation of China (Grant No. 52106099), the Natural Science Foundation of Shandong Province (Grant No. ZR2022YQ57), and the Taishan Scholars Program.

References

[1] Chong X, Zhang Y, Li E, Kim K, Ohodnicki P R, Chang C and Wang A X 2018 *ACS Sens.* **3** 230
[2] Chong X, Kim K J, Ohodnicki P R, Li E, Chang C H and Wang A X 2015 *IEEE Sens. J.* **15** 5327
[3] Benavides-Serrano A J, Mannan M S and Laird C D 2015 *J. Loss Prev. Process Ind.* **35** 339
[4] Potyrailo R A 2016 *Chem. Rev.* **116** 11877
[5] Mahapatra C 2025 *Med. Gas Res.* **15** 318
[6] Gouma P 2023 *ECS Meet. Abstr.* **MA2023-02** 2974
[7] Pan Y, Zhao J, Lu P, Sima C, Zhang W, Fu L, Liu D, Zhang J, Wu H and Dong L 2022 *Photoacoustics* **27** 100389
[8] Liu N, Mesch M, Weiss T, Hentschel M and Giessen H 2010 *Nano Lett.* **10** 2342
[9] Rodrigo D, Limaj O, Janner D, Etezadi D, de Abajo F J G, Pruneri V and Altug H 2015 *Science* **349** 165
[10] Mohammadnezhad M, Zamani-Meymian M, Vahedi M and Fallah M 2024 *Phys. Scr.* **99** 125945
[11] Zhao P, Krishnaiah K V, Guo L, Li T, Ho H L, Zhang A P and Jin W 2024 *Laser Photonics Rev.* **18** 2301285
[12] Li J, Yan H, Dang H and Meng F 2021 *Opt. Laser Technol.* **135** 106658
[13] Yan Y, Xu J, Peng Z, Ji Z, Gao Y, Jia L and Xu Q 2024 *Electronics* **13** 4800
[14] Han J, Li H, Cheng J, Ma X and Fu Y 2025 *J. Mater. Chem. C* **13** 4285
[15] Dao T D, Dubois F, Spettel J, Tortschanoff A, Fleury C, Cselyuszka N, Consani C, Nikolai A and Moridi M 2021 *OSA Continuum* **6** 1827
[16] Jha R K 2022 *IEEE Sens. J.* **22** 6
[17] Xu M, Peng B, Zhu X and Guo Y 2022 *Sensors* **22** 836
[18] Tan X, Zhang H, Li J, Wan H, Guo Q, Zhu H, Liu H and Yi F 2020 *Nat. Commun.* **11** 5245
[19] Faist J, Capasso F, Sivco D L, Sirtori C, Hutchinson A L and Cho A Y 1994 *Science* **264** 553
[20] Yao Y, Hoffman A J and Gmachl C F 2012 *Nat. Photonics* **6** 432
[21] Kumar K S, Vidhya Y E B, Selvaraj R, Seshadri S, Nagendra S M S and Vasa N J 2023 *IEEE Sens. J.* **23** 5703
[22] Sun K, Cai Y and Han Z 2022 *J. Phys. D: Appl. Phys.* **55** 025104
[23] Ma B, Huang Y, Zha W, Qin B, Qin R, Ghosh P, Kaur S, Qin M and Li Q 2022 *Nanophotonics* **11** 4115
[24] Lochbaum A, Fedoryshyn Y, Dorodnyy A, Koch U, Hafner C and Leuthold J 2017 *ACS Photonics* **4** 1371
[25] He J, Ding P, Wang J, Fan C and Liang E 2015 *Opt. Express* **23** 6083
[26] Meng L, Zhao D, Ruan Z, Li Q, Yang Y and Qiu M 2014 *Opt. Lett.* **39** 1137
[27] Hao J, Wang J, Liu X, Padilla W J, Zhou L and Qiu M 2010 *Appl. Phys. Lett.* **96** 251104
[28] Ali M O, Tait N and Gupta S 2018 *J. Opt. Soc. Am. A* **35** 119
[29] Sun M, Zhang S, Wu D and Han Z 2024 *Infrared Phys. Technol.* **137** 105132
[30] Inoue T, Zoysa M D, Asano T and Noda S 2016 *Opt. Express* **24** 15101
[31] Song F, Wu X, Liu Y and Yu K 2024 *Opt. Express* **32** 41244
[32] Zhou J, Wang B and Zhao C 2024 *IEEE Sens. J.* **24** 20468
[33] Lochbaum A, Dorodnyy A, Koch U, Koepfli S M, Volk S, Fedoryshyn Y, Wood V and Leuthold J 2020 *Nano Lett.* **20** 4169
[34] Li X, Maqbool E and Han Z 2023 *Opt. Express* **31** 20338
[35] Yang S, He M, Hong C, Nordlander J, Maria J, Caldwell J D and Ndukaife J C 2024 *Optica* **11** 305
[36] Sun K, Sun M, Ma Y, Shi Y and Han Z 2023 *Int. Commun. Heat Mass Transf.* **143** 106728
[37] Zhu H, Luo H, Li Q, Zhao D, Cai L, Du K, Xu Z, Ghosh P and Qiu M 2018 *Opt. Lett.* **43** 5230
[38] Qiu Q, Zhou D, Zhang J, Tan C, Xu Q, Zhang Z, Wen Z, Sun Y, Dai N and Hao J 2023 *Opt. Lett.* **48** 6000
[39] Yang Z, IsHii S, Yokoyama T, Dao T D, Sun M G, Pankin P S, Timofeev I V, Nagao T and Chen K P 2017 *ACS Photonics* **4** 2212
[40] Pühringer G, Brandner D, Tischler C, Jannesari R, Grille T, Stocker G, Putz V and Jakoby B 2023 *Micro Nano Eng.* **19** 100209
[41] Amotchkina T, Trubetskov M, Hahner D and Pervak V 2020 *Appl. Opt.* **59** A40
[42] Li L and Hao H 2022 *Sci. Rep.* **12** 14921
[43] Giteau M, Conrads L, Mathwieser A, Schmitt R, Wuttig M, Taubner T and Papadakis G T 2024 *Laser Photonics Rev.* **19** 2401438
[44] Zhang Z M, Wu X and Fu C 2020 *J. Quant. Spectrosc. Radiat. Transfer* **245** 106904
[45] Hu J, Yao E, Xie W, Liu W, Li D, Lu Y and Zhan Q 2019 *Opt. Express* **27** 18642